Real-time MBDi-RPA using methyl-CpG binding protein 2: A real-time detection method for simple and rapid estimation of CpG methylation status

（DNA メチル化を迅速かつ簡便に評価するための MeCP2 を用いたリアルタイム MBDi-RPA 法）

申 請 者　弘前大学大学院医学研究科
病態制御科学領域 呼吸病態内科学教育研究分野

氏　　名　石戸谷　美奈

指導教授　田坂　定智

Abstract

Background

Analysis of CpG methylation is informative for cancer diagnosis. Previously, we developed a novel method to discriminate CpG methylation status in target DNA by blocking recombinase polymerase amplification (RPA), an isothermal DNA amplification technique, using methyl-CpG binding domain (MBD) protein 2 (MBD2). The method was named MBD protein interference-RPA (MBDi-RPA). In this study, MBDi-RPA was performed using methyl-CpG binding protein 2 (MeCP2), another MBD family protein, as the blocking agent.

Results

MBDi-RPA using MeCP2 detected low levels of CpG methylation, showing that it had higher sensitivity than MBDi-RPA using MBD2. We also developed real-time RPA, which enabled rapid analysis of DNA amplification without the need for laborious agarose gel electrophoresis and used it in combination with MBDi-RPA. We termed this method real-time MBDi-RPA. The method using MeCP2 could determine the abundance ratio of CpG-methylated target DNA simply and rapidly, although highly sensitive detection was challenging.

Significance and Novelty

Real-time MBDi-RPA using MeCP2 could be potentially useful for estimating CpG methylation status in target DNA prior to more detailed analyses.

Keywords

Methylation; CpG; MBD; MeCP2; RPA; MBDi-RPA

1. Introduction

Aberrant CpG methylation is observed in various diseases [1]. Methylation of CpG islands, which are DNA regions containing abundant CpG sites, is associated with many malignancies including liver, lung, colon, and blood cancers [2-6]. CpG methylation analysis is thus useful for the diagnosis of tumors and the design of medical treatments [7, 8].

Several methods for detecting CpG methylation status have been developed. Bisulfite treatment followed by methylation-specific PCR (MSP) [9] or pyrosequencing [10, 11] are bisulfite-based methods for the evaluation of CpG methylation. Enzyme-based methods rely on methylation-sensitive restriction enzyme(s) (MRE). In these methods, DNA regions that are not cleaved by MREs (i.e., CpG-methylated regions) are analyzed by PCR or next generation sequencing (NGS) for genome wide analysis [12]. Immunoprecipitation-based methods, such as methylated DNA immunoprecipitation (MeDIP), can enrich DNA regions including methylated CpG sites in the genome. These methods use methyl-CpG binding domain (MBD) proteins, such as MBD2 and methyl-CpG binding protein 2 (MeCP2), to capture methylated CpG [13, 14]. Immunoprecipitated DNA can be analyzed by PCR or NGS. Among these methods, bisulfite treatment followed by MSP is the most widely used technique. However, it requires bisulfite treatment and the design of primers specific for bisulfite-converted DNA. In addition, bisulfite treatment is time-consuming and damages DNA [15].

Recombinase polymerase amplification (RPA) is an isothermal method that amplifies target DNA at 37°C for 10–20 min [16]. We previously developed a bisulfite treatment-free method for analyzing CpG methylation status in template DNA in which RPA is used for DNA amplification [17]. In this method, named MBD protein interference-RPA (MBDi-RPA), target DNA is amplified by RPA in the presence of MBD proteins (e.g., MBD2, Fig. 1). If the CpG sites

of target DNA are methylated, MBD proteins will bind to the sites and block extension of DNA polymerases from primers. Although this method is simple and time-efficient, the number of CpG-methylated sites necessary for blocking extension of DNA polymerases (i.e., DNA amplification) remains unclear.

In this study, we examined the reaction properties of MBD proteins in MBDi-RPA. We found that MeCP2 was more suitable for MBDi-RPA than MBD2. We also established a novel real-time RPA protocol to evaluate target DNA amplification simply and rapidly and combined it with MBDi-RPA. This method was termed real-time MBDi-RPA. The present results demonstrate that real-time MBDi-RPA is a simple method for estimating CpG methylation status in target DNA.

2. Experimental section

2.1. Oligonucleotides

Oligodeoxyribonucleotides (ODNs) were chemically synthesized (Eurofins Genomics, Tokyo, Japan) and used as primers. Dual-labeled oligoribonucleotides (ORNs) were chemically synthesized and purified by high-performance liquid chromatography (FASMAC, Kanagawa, Japan). The ODNs and ORNs used in this study are listed in Table S1.

2.2 Preparation of template DNA (plasmid DNA and genomic DNA)

Template DNA including 5, 10, or 20 CpG sites (CpG_5, CpG_10, and CpG_20) was generated by a DNA synthesis service (Eurofins Genomics). Template DNA including 1 CpG site (CpG_1) was prepared as described previously [17]. DNA was CpG-methylated using the CpG methyltransferase M.SssI (#M0226, New England Biolabs, Ipswich, MA, USA) as described previously [17]. CpG-methylated and -unmethylated CpG_2 was previously prepared [17]. HCT116 genomic DNA (gDNA) prepared previously [17] was used in this study. EpiScope Methylated HCT116 gDNA (highly methylated *in vitro*, #3522, Takara Bio, Shiga, Japan) and EpiScope Unmethylated HCT116 DKO gDNA (CpG-methylation: < 5%, #3521, Takara Bio) were used as CpG-methylated and -unmethylated gDNA, respectively. We calculated the copy number of a target DNA from the length and concentration of DNA.

2.3. MBD proteins

The MBD2 protein (1 μg/μL) in the EpiXplore Methylated DNA Enrichment Kit (#631963, Takara Bio) was used for MBDi-RPA. The MeCP2 protein (4 μg/μL) was purchased from Diagenode (#C02020012, Seraing, Belgium). For MBDi-RPA, the MeCP2 protein was adjusted to a

concentration of 1 μg/μL with phosphate buffered saline (PBS) containing 10% glycerol (v/v).

2.4. MBDi-RPA reactions

RPA was performed using a TwistAmp Basic Kit (#TABAS03KIT, TwistDx, Maidenhead, UK) as described previously [17]. Briefly, a pre-reaction mixture was prepared by adding 29.5 μL of rehydration buffer, 2.5 μL of each primer (10 μM), and 5.5 μL of nuclease-free water to one freeze-dried component. An aliquot (16 μL) of the pre-reaction mixture was mixed with MBD2 (0.5 μg) or MeCP2 (0.5 and 2 μg for Figs. 3 and 2, respectively), template DNA [plasmid DNA (1 pg) or gDNA (20 ng)], and nuclease-free water, resulting in a final volume of 19 μL. After incubation at 37°C for 10 min, 1 μL of MgOAc (280 mM) was added to the mixture (20 μL in total). The reaction mixture was further incubated at 37°C for 10–30 min. RPA products were purified using the FastGene PCR/Gel DNA Purification Kit (#FG-91302, Nippon Genetics, Tokyo, Japan) if necessary and electrophoresed on 2% agarose gels. As to Fig. S3, RPA products were subjected to real-time PCR as described below.

2.5. Real-time PCR of RPA products

RPA products were diluted with distilled water (1,000-fold dilution) and used for real-time PCR with THUNDERBIRD Next SYBR qPCR Mix (#QPX-201, Toyobo, Osaka, Japan) according to the manufacturer's instructions. Briefly, 5 μL of THUNDERBIRD Next SYBR qPCR Mix, 0.3 μL of each primer (10 μM), and 2 μL of diluted RPA sample were mixed to a final volume of 10 μL. Real-time PCR was performed using the CFX Connect Real-Time PCR Detection System (#1855201J1, Bio-Rad Laboratories, Hercules, CA, USA). The PCR cycles were as follows: hold 95°C for 30 sec, 40 cycles of 95°C for 5 sec and 60°C for 10 sec.

2.6. DNA sequencing analysis

DNA sequencing analysis was performed by a DNA sequencing service (Eurofins Genomics). DNA sequencing data were analyzed with SnapGene Viewer (https://www.snapgene.com/snapgene-viewer).

2.7. Real-time RPA/MBDi-RPA

A pre-reaction mixture for RPA was prepared as described above. An aliquot (16 μL) of the pre-reaction mixture was mixed with 0.4 μL or 1 μL of a dual-labeled ORN (10 μM), 0.5 μL of Thermostable RNaseH (#M0523, New England Biolabs), and template DNA [plasmid DNA (1 pg) or gDNA (32–0.02 ng)] to a final volume of 19 μL in Multiplate 96-Well PCR Plates (#MLL9651, Bio-Rad). After adding 1 μL of MgOAc (280 mM), the reaction mixture was incubated at room temperature for 4 min, mixed, and then incubated for 30 min using the MiniOpticon Real-Time PCR Detection System (#CFD-3120J1, Bio-Rad Laboratories). For real-time MBDi-RPA, 0.5 μg (Fig. 5C) or 1 μg (others) of MeCP2 was additionally added to the reaction mixture while still maintaining a final volume of 19 μL. Bovine serum albumin (BSA; supplied as a restriction enzyme product supplement by Takara Bio) was added instead of MeCP2 as a negative control protein. The reaction mixture was then incubated at 37°C for 10 min before addition of MgOAc.

3. Results and discussion

3.1. Discrimination of CpG methylation status by MBDi-RPA using different MBD proteins

MBDi-RPA using MBD2 can discriminate the CpG methylation status of target DNA containing 28 methylated CpG sites [17]. We examined the number of methylated CpG sites in the target DNA required to block DNA amplification. To this end, we prepared template DNA containing 20, 10, 5, 2, or 1 CpG site(s) between primer annealing sites (CpG_20, CpG_10, CpG_5, CpG_2, or CpG_1; Figs. 2A and S1). As shown in Fig. 2B and C, methylation of CpG_20 and CpG_10 suppressed DNA amplification completely and marginally, respectively, in the presence of MBD2. By contrast, MBD2 did not affect amplification of methylated CpG_5. These results suggest that ≥ 20 sites of methylated CpG are required to completely block DNA amplification by MBDi-RPA using MBD2, which is consistent with previous results [17].

The MBD protein family consists of seven members, MBD1–6 and MeCP2 [18,19]. Among them, MBD2 and MeCP2 have been used to capture CpG-methylated DNA [13,14]. We tested the efficacy of MBDi-RPA using MeCP2 and found that DNA amplification was completely suppressed when CpG_20, CpG_10, CpG_5, and CpG_2 were methylated (Fig. 2D). DNA amplification of methylated CpG_1 was slightly suppressed in the presence of MeCP2 (Fig. 2D). To confirm the CpG methylation-specific suppression event, we used a mixture of CpG-unmethylated CpG_20 and CpG-methylated CpG_10, or CpG-methylated CpG_20 and CpG-unmethylated CpG_10, as the template (Fig. 2E). RPA amplified the target regions even in the presence of MeCP2. DNA sequencing analysis of the amplicons confirmed that MeCP2 suppressed DNA amplification only from CpG-methylated templates (Fig. 2F). These results demonstrate that (1) MeCP2 specifically binds to CpG-methylated templates and suppresses DNA amplification in MBDi-RPA, and (2) MBDi-RPA using MeCP2 is more sensitive for discriminating CpG

methylation status than MBDi-RPA with MBD2.

We evaluated the efficacy of MBDi-RPA using MeCP2 with gDNA extracted from human cells. In this experiment, we analyzed the *CDKN2A* genes (*p14ARF* and *p16INK4A*) of the human colorectal carcinoma cell line HCT116, which are CpG-methylated on one allele and unmethylated on the other one (Fig. 3A) [20]. The methylated and unmethylated alleles can be distinguished by the presence/absence of single-nucleotide mutations (Figs. 3A and S2). As shown in Fig. 3B–E, MBDi-RPA amplified the target regions of the *p14ARF* and *p16INK4A* genes even in the presence of MeCP2. DNA sequencing analysis confirmed DNA amplification from the unmethylated alleles (Fig. 3C and E). The results suggest that MBDi-RPA using MeCP2 distinguishes the CpG methylation status of gDNA extracted from cells as well as artificially prepared template DNA.

We showed that MBDi-RPA using MBD2 can estimate CpG methylation status when ≥ 20 CpG sites are methylated (Fig. 2C). However, MBDi-RPA using MeCP2 can determine the CpG methylation status even when only 2 CpG sites are methylated (Fig. 2D). Although both MBD2 and MeCP2 bind to methylated CpGs, their binding modes are different. MeCP2 tightly binds to a single methylation site [21] and contains a transcriptional regulatory domain that plays an important role in the regulation of gene expression [22]. By contrast, MBD2 does not have such domains. In addition, MeCP2 has conformational adaptability and can change DNA conformation when binding to CpG-methylated DNA [23]. These differences may affect the suppression of DNA polymerase-mediated extension in RPA. Alternatively, quality, structure, or fused epitope-tags of the recombinant proteins (MBD2 or MeCP2) may affect the suppression efficiency. Many of the properties of recombinant proteins are not disclosed by their manufacturers, preventing a detailed discussion of their properties. However, under the present experimental conditions, MBDi-RPA using MeCP2 showed higher sensitivity for evaluating CpG methylation (Fig. 2). On the other

hand, if MBDi-RPA targets a region possessing ≥ 20 CpG sites, MBD2 and MeCP2 will yield comparable results. In fact, when we analyzed *p14ARF* and *p16INK4A* regions (≥ 20 CpG sites, each) with HCT116 gDNA by MBDi-RPA using MBD2, the unmethylated alleles were selectively amplified [17]. Therefore, depending on the number of CpGs in a target region, either MBD2 or MeCP2 should be used for MBDi-RPA.

3.2. Establishment of a real-time RPA system

Although MBDi-RPA is a useful method for evaluating CpG methylation status, the agarose gel electrophoresis step remains laborious. To overcome this problem, we attempted to detect DNA amplification by RPA using real-time PCR. As shown in Fig. S3, real-time PCR detected specific DNA amplification by RPA. When the RPA products of methylated CpG_2 template DNA were subjected to real-time PCR, an approximately 2-cycle delay of fluorescent amplification (equivalent to a 75% reduction in DNA amplification) was observed when the amplification reaction contained MeCP2 (Fig. S3). Such a delay was not observed for the RPA products of unmethylated CpG_2 template DNA. These results are consistent with the results shown in Fig. 2D. However, real-time PCR is still time-consuming. We therefore attempted to establish a novel real-time RPA detection system that does not require agarose gel electrophoresis or real-time PCR. We previously showed that an ORN, a short RNA, hybridizes to its complementary sequence and blocks DNA amplification in RPA reactions (Fig. 4A) [17]. Based on this property, we tested the use of a dual-labeled ORN as a probe (Fig. 4B, left panel). In this experiment, RPA is performed in the presence of a dual-labeled ORN and RNase H. If the dual-labeled ORN hybridizes to its complementary sequence in an amplified region, RNase H will specifically cleave (degrade) the ORN in the ORN/DNA hybrid, resulting in the emission of fluorescence. Because the hybridized

ORN is degraded, DNA extension is not blocked.

We first tested the feasibility of this detection system using HCT116 gDNA as the template DNA. Because HCT116 cells harbor a *KRAS* G13D mutation, we designed two dual-labeled ORNs, ORN_KRAS_G13D_Probe and ORN_EGFR_CG5_10_20_Probe; the former is completely complementary to the G13D mutation sequence of the *KRAS* gene in HCT116 gDNA (Fig. S4A–C and Table S1), and the latter is complementary to the artificial templates CpG_5, CpG_10, and CpG_20 (Table S1). When the *KRAS* gene was amplified with HCT116 gDNA, the ORN_KRAS_G13D_Probe partially inhibited the target DNA amplification (Fig. S4D). The suppression was restored in the presence of RNase H (Fig. S4D), consistent with the schematic diagram in Fig. 4B (left panel). We next measured the fluorescence emitted from the cleavage of the dual-labeled ORN. Fluorescence signals were detected when the *KRAS* gene was amplified in the presence of ORN_KRAS_G13D_Probe but not ORN_EGFR_CG5_10_20_Probe (an irrelevant probe) (Fig. S4E). These results indicate that a dual-labeled ORN in the ORN/DNA hybrid is specifically cleaved (degraded), and target amplification can be detected by monitoring fluorescence emission.

Next, we performed real-time RPA with the template CpG_10 and ORN_EGFR_CG5_10_20_Probe (Fig. S5A). ORN_EGFR_CG5_10_20_Probe but not ORN_KRAS_G13D_Probe detected amplification of CpG_10 (Fig. 4C), confirming the target selectivity of real-time RPA. As shown in Fig. 4D, fluorescence was emitted in a DNA concentration-dependent manner [25–0.2 pg (8.3×10^6–6.7×10^4 copies)]. Target-specific amplification was confirmed by electrophoresis (Fig. S5B). Fluorescence detection was achieved even with lower amounts of CpG_10 [0.2–0.008 pg (6.7×10^4–2.7×10^3 copies), Fig. 4E]. Taken together, the results indicate that real-time RPA using the combination of a dual-labeled ORN and

RNase H is feasible to detect amplification of target DNA in a sequence-specific manner. Considering the signal intensity of 2.7×10^3 copies (Fig. 4E), we speculate that this system can detect $\geq 5 \times 10^2$ copies (further 5-fold dilution) of purified plasmid DNA. In addition, because amplification of CpG_10 and *KRAS* was selectively detected by each dual-labeled ORN, this real-time detection system can distinguish between widely different sequences. On the other hand, we found that ORN_KRAS_G13D_Probe binds to the *KRAS* G13D sequence with greater affinity than to the WT sequence (Fig. S6), which is consistent with the higher complementarity. These results imply that discrimination of a single nucleotide difference is feasible, although additional technical improvement will be necessary to achieve higher specificity.

3.3. Real-time MBDi-RPA for analyzing CpG methylation status

Next, we examined the feasibility of real-time MBDi-RPA (Fig. 4B, right panel). We first investigated whether addition of additional proteins such as MeCP2 affect the real-time RPA reaction. To test this, we performed real-time RPA in the presence of an irrelevant protein, BSA. As shown in Fig. S7, fluorescence emission was reduced to some extent in the presence of BSA, suggesting that the addition of irrelevant proteins partially inhibits the real-time RPA reaction. Therefore, to interpret the results correctly, negative control reactions should be performed with irrelevant proteins such as BSA. When real-time MBDi-RPA was performed with CpG-methylated CpG_5 as the template DNA, MeCP2, but not BSA, completely inhibited fluorescence emission (target amplification) (Fig. 4F and G). When a mixture of CpG-methylated and -unmethylated CpG_5 (1:1 ratio) was used as template DNA, fluorescence emission was partially decreased in the presence of MeCP2 (Fig. 4H). These results are consistent with those of MBDi-RPA (Fig. 2E) and confirm that real-time MBDi-RPA is feasible for evaluating CpG methylation status rapidly.

We next examined the practical utility of real-time RPA/MBDi-RPA using gDNA. To this end, we designed a dual-labeled ORN (ORN_p14_Probe) targeting the *p14ARF* gene (Fig. S8A). Real-time RPA using the ORN_p14_Probe detected amplification of the *p14ARF* gene in reactions containing 32–0.5 ng (10,666–167 copies of the gene) of HCT116 gDNA in a dose-dependent manner (Fig. 5A and B). Although the *p14ARF* gene was detected in 0.2 ng (66 copies of the gene) of the gDNA, the amplification signal was weak and could not be discriminated from the amplification signal of 0.02 ng (six copies of the gene) of gDNA (Fig. S8B). Therefore, the *p14ARF* gene may not be detected accurately when low amounts of gDNA are used (< 0.2 ng). Thus, for the detection of a single copy gene, the limit of detection sensitivity of real-time RPA using gDNA would be 0.5–0.2 ng of gDNA (167–66 copies of a target gene).

We next tested real-time MBDi-RPA with HCT116 gDNA. As shown in Fig. 5C, fluorescence emission decreased in the presence of MeCP2 probably due to suppression of amplification of the CpG-methylated *p14ARF* DNA. Real-time MBDi-RPA can evaluate the presence of CpG methylation in target DNA simply and rapidly when ≥ 50% of the target DNA is CpG-methylated. When 20 ng of HCT116 gDNA was used as a template DNA, 0.2–1 μg of MeCP2 strongly suppressed amplification of the CpG-methylated *p14ARF* while 2 μg suppressed it nearly completely (Fig. S8C and D). Therefore, 1–2 μg of MeCP2 would appear to the optimal amount for real-time MBDi-RPA with 20 ng of gDNA. Lastly, we examined the sensitivity of CpG-methylated DNA detection by real-time MBDi-RPA using model gDNA. To this end, we mixed commercially available CpG-methylated and unmethylated gDNA at different ratios (Fig. 5D). Real-time MBDi-RPA discriminated between 100%, 90%, 30%, and 0% CpG-methylated DNA containing the *p14ARF* gene (Fig. 5E). Fluorescent emission decreased in proportion to the amounts of CpG-methylated DNA (Fig. 5F). Thus, real-time MBDi-RPA is potentially useful for

obtaining rough estimates of the abundance ratio of CpG-methylated target DNA (i.e., at a level of ca. 10%). It is of note that amplification of CpG-methylated gDNA in reactions containing 100% of this template was not suppressed completely by MeCP2 (Fig. 5E). In this regard, because 1 μg of MeCP2 did not completely suppress the amplification of the CpG-methylated *p14ARF* (Fig. S8D), amplification of methylated *p14ARF* would be detected. Therefore, although 1 μg of MeCP2 may be a practical amount for obtaining a rough estimate of the abundance ratio of CpG-methylated target DNA, more of this protein is necessary to completely suppress amplification (fluorescent emission) when gDNA is used as the template DNA.

Real-time MBDi-RPA using a dual-labeled ORN enables evaluation of the CpG methylation status in a short time without electrophoresis (Figs. 4 and 5). Before the development of this system, we considered using TwistAmp exo (TwistDX), a commercially available real-time RPA reagent. However, there are few commercial companies that can synthesize an exo probe, a specific probe for TwistAmp exo, and we cannot design an ideal exo probe. We therefore designed a different real-time RPA system and demonstrated that it has certain advantages over the exo probe system. First, synthesis of an exo probe is more expensive than that of a dual-labeled ORN. Second, the design of an exo probe is complex. Third, a dual-labeled ORN can potentially distinguish a single-nucleotide difference. The properties of the real-time methods for the detection of CpG-methylated DNA are listed in Table 1 [24-30]. Real-time MBDi-RPA does not require time-consuming bisulfite treatment or restriction enzyme digestion. However, in its current form, real-time RPA/MBDi-RPA does not detect a target DNA/CpG methylation status with high sensitivity. Therefore, its use will probably be limited to obtaining a rough estimate of CpG methylation status in target DNA before performing more detailed analyses. In the present study, we demonstrated that real-time MBDi-RPA was performant in estimating CpG methylation status

in proof-of-concept studies using model DNA. An important aim of future research will be to evaluate whether it can be used to evaluate the CpG methylation status of DNA of biological origin under various physiological conditions. Additional assessments and technical improvements will also be necessary before this novel system can be used for the real-time measurement of CpG methylation.

4. Conclusions

In this study, we found that MBDi-RPA using MeCP2 can discriminate target DNAs containing small numbers of CpG methylation sites. Therefore, MBDi-RPA using MeCP2 is more sensitive for evaluating CpG methylation status of target templates than MBDi-RPA using MBD2. We also established a real-time MBDi-RPA system that can analyze CpG methylation status within 30 min. In its current form, this method is potentially useful for obtaining a rough estimate of CpG methylation status in target DNA prior to more detailed analyses. CpG methylation of promoter regions in tumor suppressor genes, such as *CDKN2A*, *MLH1*, *RB1*, and *BRCA1*, is involved in cancer development [31-33]. By contrast, CpG demethylation of promoter regions in oncogenes, such as *CHRNB4* and *S100A4*, is also involved in cancer development [34, 35]. Thus, detection of CpG methylation and demethylation events is informative for early cancer diagnosis and prognosis prediction [36-39]. The clinical application of this method using biopsy specimens would be an interesting future study.

Acknowledgments

We thank Shoko Nagata for technical assistance. This work was supported by a Grant-in-Aid for Scientific Research (B) (#21H02457) (T.F.) from the Ministry of Education, Culture, Sports, Science and Technology of Japan.

Author contributions

T.F. conceived and supervised the project. M.I. and T.F. designed and performed the experiments. S.T. and H.F. provided critical advice. M.I., T.F., and H.F. wrote the manuscript.

Competing interests statement

T.F. and H.F. have filed patent applications for MBDi-RPA as follows: name: Method for detecting target nucleic acid, method for detecting molecules with nucleic acid binding ability, and method for evaluating nucleic acid binding ability. Japanese Patent Application No. 2021-552470; status: filed.

References

[1] K. Skvortsova, C. Stirzaker, P. Taberlay, The DNA methylation landscape in cancer, Essays Biochem. 63(6) (2019) 797-811.

[2] Y. Kondo, Y. Kanai, M. Sakamoto, M. Mizokami, R. Ueda, S. Hirohashi, Genetic instability and aberrant DNA methylation in chronic hepatitis and cirrhosis-A comprehensive study of loss of heterozygosity and microsatellite instability at 39 loci and DNA hypermethylation on 8 CpG islands in microdissected specimens from patients with hepatocellular carcinoma, Hepatology 32(5) (2000) 970-979.

[3] C.A. Eads, R.V. Lord, S.K. Kurumboor, K. Wickramasinghe, M.L. Skinner, T.I. Long, J.H. Peters, T.R. DeMeester, K.D. Danenberg, P.V. Danenberg, P.W. Laird, K.A. Skinner, Fields of aberrant CpG island hypermethylation in Barrett's esophagus and associated adenocarcinoma, Cancer Res. 60(18) (2000) 5021-5026.

[4] M. Guo, M.G. House, C. Hooker, Y. Han, E. Heath, E. Gabrielson, S.C. Yang, S.B. Baylin, J.G. Herman, M.V. Brock, Promoter hypermethylation of resected bronchial margins: a field defect of changes?, Clin. Cancer Res. 10(15) (2004) 5131-5136.

[5] T. Maekita, K. Nakazawa, M. Mihara, T. Nakajima, K. Yanaoka, M. Iguchi, K. Arii, A. Kaneda, T. Tsukamoto, M. Tatematsu, G. Tamura, D. Saito, T. Sugimura, M. Ichinose, T. Ushijima, High levels of aberrant DNA methylation in Helicobacter pylori-infected gastric mucosae and its possible association with gastric cancer risk, Clin. Cancer Res. 12(3) (2006) 989-995.

[6] L. Shen, Y. Kondo, G.L. Rosner, L. Xiao, N.S. Hernandez, J. Vilaythong, P.S. Houlihan, R.S. Krouse, A.R. Prasad, J.G. Einspahr, J. Buckmeier, D.S. Alberts, S.R. Hamilton, J.P. Issa, MGMT promoter methylation and field defect in sporadic colorectal cancer, J. Natl. Cancer Inst. 97(18) (2005) 1330-1338.

[7] P.A. Jones, J.P. Issa, S. Baylin, Targeting the cancer epigenome for therapy, Nat. Rev. Genet. 17(10) (2016) 630-641.

[8] A.P. Feinberg, B. Tycko, The history of cancer epigenetics, Nat. Rev. Cancer 4(2) (2004) 143-153.

[9] J.G. Herman, J.R. Graff, S. Myohanen, B.D. Nelkin, S.B. Baylin, Methylation-specific PCR: a novel PCR assay for methylation status of CpG islands, Proc. Natl. Acad. Sci. U. S. A. 93(18) (1996) 9821-9826.

[10] J. Tost, J. Dunker, I.G. Gut, Analysis and quantification of multiple methylation variable positions in CpG islands by Pyrosequencing, BioTechniques 35(1) (2003) 152-156.

[11] E. Yamamoto, M. Toyota, H. Suzuki, Y. Kondo, T. Sanomura, Y. Murayama, M. Ohe-Toyota, R. Maruyama, M. Nojima, M. Ashida, K. Fujii, Y. Sasaki, N. Hayashi, M. Mori, K. Imai, T. Tokino, Y. Shinomura, LINE-1 hypomethylation is associated with increased CpG island methylation in Helicobacter pylori-related enlarged-fold gastritis, Cancer Epidemiol Biomarkers Prev. 17(10) (2008) 2555-2564.

[12] A.K. Maunakea, R.P. Nagarajan, M. Bilenky, T.J. Ballinger, C. D'Souza, S.D. Fouse, B.E. Johnson, C.B. Hong, C. Nielsen, Y.J. Zhao, G. Turecki, A. Delaney, R. Varhol, N. Thiessen, K. Shchors, V.M. Heine, D.H. Rowitch, X.Y. Xing, C. Fiore, M. Schillebeeckx, S.J.M. Jones, D. Haussler, M.A. Marra, M. Hirst, T. Wang, J.F. Costello, Conserved role of intragenic DNA methylation in regulating alternative promoters, Nature 466(7303) (2010) 253-257.

[13] S. Li, T.O. Tollefsbol, DNA methylation methods: Global DNA methylation and methylomic analyses, Methods 187 (2021) 28-43.

[14] D. Serre, B.H. Lee, A.H. Ting, MBD-isolated Genome Sequencing provides a high-throughput and comprehensive survey of DNA methylation in the human genome, Nucleic Acids

Res. 38(2) (2010) 391-399.

[15] N. Olova, F. Krueger, S. Andrews, D. Oxley, R.V. Berrens, M.R. Branco, W. Reik, Comparison of whole-genome bisulfite sequencing library preparation strategies identifies sources of biases affecting DNA methylation data, Genome Biol. 19(1) (2018) 33.

[16] O. Piepenburg, C.H. Williams, D.L. Stemple, N.A. Armes, DNA detection using recombination proteins, PLoS Biol. 4(7) (2006) e204.

[17] T. Fujita, S. Nagata, H. Fujii, Protein or ribonucleoprotein-mediated blocking of recombinase polymerase amplification enables the discrimination of nucleotide and epigenetic differences between cell populations, Commun. Biol. 4(1) (2021) 988.

[18] Q. Du, P.L. Luu, C. Stirzaker, S.J. Clark, Methyl-CpG-binding domain proteins: readers of the epigenome, Epigenomics 7(6) (2015) 1051-1073.

[19] H.I. Baymaz, A. Fournier, S. Laget, Z. Ji, P.W. Jansen, A.H. Smits, L. Ferry, A. Mensinga, I. Poser, A. Sharrocks, P.A. Defossez, M. Vermeulen, MBD5 and MBD6 interact with the human PR-DUB complex through their methyl-CpG-binding domain, Proteomics 14(19) (2014) 2179-2189.

[20] T. Fujita, M. Yuno, H. Fujii, Allele-specific locus binding and genome editing by CRISPR at the p16INK4a locus, Sci. Rep. 6 (2016) 30485.

[21] X.S. Nan, P. Tate, E. Li, A. Bird, DNA methylation specifies chromosomal localization of MeCP2, Mol. Cell. Biol. 16(1) (1996) 414-421.

[22] R.I.D. Wakefield, B.O. Smith, X.S. Nan, A. Free, A. Soteriou, D. Uhrin, A.P. Bird, P.N. Barlow, The solution structure of the domain from MeCP2 that binds to methylated DNA, J. Mol. Biol. 291(5) (1999) 1055-1065.

[23] T. Clouaire, I. Stancheva, Methyl-CpG binding proteins: specialized transcriptional repressors

or structural components of chromatin?, Cell. Mol. Life Sci. 65(10) (2008) 1509-1522.

[24] U. Lehmann, B. Hasemeier, R. Lilischkis, H. Kreipe, Quantitative analysis of promoter hypermethylation in laser-microdissected archival specimens, Lab. Invest. 81(4) (2001) 635-638.

[25] C. Gebhard, L. Schwarzfischer, T.H. Pham, R. Andreesen, A. Mackensen, M. Rehli, Rapid and sensitive detection of CpG-methylation using methyl-binding (MB)-PCR, Nucleic Acids Res. 34(11) (2006) e82.

[26] A. Schumacher, A. Petronis, Epigenetics of complex diseases: from general theory to laboratory experiments, Curr. Top. Microbiol. Immunol. 310 (2006) 81-115.

[27] E. Olkhov-Mitsel, B. Bapat, Strategies for discovery and validation of methylated and hydroxymethylated DNA biomarkers, Cancer Med. 1(2) (2012) 237-260.

[28] H.G. Hernandez, M.Y. Tse, S.C. Pang, H. Arboleda, D.A. Forero, Optimizing methodologies for PCR-based DNA methylation analysis, BioTechniques 55(4) (2013) 181-197.

[29] J. Wang, Y. Xia, L. Li, D. Gong, Y. Yao, H. Luo, H. Lu, N. Yi, H. Wu, X. Zhang, Q. Tao, F. Gao, Double restriction-enzyme digestion improves the coverage and accuracy of genome-wide CpG methylation profiling by reduced representation bisulfite sequencing, BMC Genomics 14 (2013) 11.

[30] S. Kurdyukov, M. Bullock, DNA methylation analysis: Choosing the right method, Biology (Basel) 5(1) (2016) 3.

[31] M. Esteller, Molecular origins of cancer: Epigenetics in cancer, N. Engl. J. Med. 358(11) (2008) 1148-1159.

[32] P.A. Jones, S.B. Baylin, The epigenomics of cancer, Cell 128(4) (2007) 683-692.

[33] R. Taby, J.P.J. Issa, Cancer epigenetics, CA Cancer J. Clin. 60(6) (2010) 376-392.

[34] D.B. Scherf, N. Sarkisyan, H. Jacobsson, R. Claus, J.L. Bermejo, B. Peil, L. Gu, T. Muley, M.

Meister, H. Dienemann, C. Plass, A. Risch, Epigenetic screen identifies genotype-specific promoter DNA methylation and oncogenic potential of CHRNB4, Oncogene 32(28) (2013) 3329-3338.

[35] R. Xie, D.S. Loose, G.L. Shipley, S. Xie, R.L. Bassett, Jr., R.R. Broaddus, Hypomethylation-induced expression of S100A4 in endometrial carcinoma, Mod. Pathol. 20(10) (2007) 1045-1054.

[36] P.W. Laird, The power and the promise of DNA methylation markers, Nat. Rev. Cancer 3(4) (2003) 253-266.

[37] H. Shi, M.X. Wang, C.W. Caldwell, CpG islands: their potential as biomarkers for cancer, Expert Rev. Mol. Diagn. 7(5) (2007) 519-531.

[38] A. Aggerholm, M.S. Holm, P. Guldberg, L.H. Olesen, P. Hokland, Promoter hypermethylation of $p15^{INK4B}$, HIC1, CDH1, and ER is frequent in myelodysplastic syndrome and predicts poor prognosis in early-stage patients, Eur. J. Haematol. 76(1) (2006) 23-32.

[39] J.R. Fischer, U. Ohnmacht, N. Rieger, M. Zemaitis, C. Stoffregen, M. Kostrzewa, E. Buchholz, C. Manegold, H. Lahm, Promoter methylation of RASSF1A, RARbeta and DAPK predict poor prognosis of patients with malignant mesothelioma, Lung Cancer 54(1) (2006) 109-116.

Table and figure legends

Table 1. Comparison of real-time methods for the detection of CpG-methylated DNA

Fig. 1. MBDi-RPA discriminates CpG methylation status.

Schematic diagram of MBDi-RPA using MBD proteins as blocking reagents. MBD proteins such as MBD2 bind to methylated CpG sites (stars) in target sequences, thereby inhibiting extension by DNA polymerases (DNA amplification). MBDi-RPA can be used to discriminate CpG methylation status in target sequences.

Fig. 2. MBDi-RPA using different MBD proteins.

(**A**) Schematic diagram of template DNA. Detailed sequences are shown in Fig. S1. (**B**) Preparation of CpG-methylated or -unmethylated template DNA. (**C**) Results of MBDi-RPA using MBD2 proteins. M, molecular weight marker. Amplified target DNA is indicated by arrowheads. (**D** and **E**) Results of MBDi-RPA using MeCP2 proteins. (**F**) Results of DNA sequencing analysis. RPA and MBDi-RPA amplicons shown in (**E**) were sequenced using a forward primer.

Fig. 3. MBDi-RPA using MeCP2 to discriminate CpG methylation status in HCT116 gDNA.

(**A**) Schematic diagram of the human *CDKN2A* (*p14ARF* and *p16INK4A*) genes in HCT116 cells. (**B** and **D**) Results of MBDi-RPA targeting *p14ARF* (**B**) and *p16INK4A* (**D**). Amplified target DNA is indicated by arrowheads. M, molecular weight marker. (**C** and **E**) Results of DNA sequencing analysis. RPA and MBDi-RPA amplicons shown in (**B**) and (**D**) were sequenced using reverse primers.

Fig. 4. Real-time RPA and MBDi-RPA using a dual-labeled ORN.

(**A**) Schematic diagram of ORNi-RPA, a blocking RPA for inhibiting DNA amplification by an ORN complementary to a target sequence. DNA extension is arrested by the hybridized ORN. (**B**) Schematic diagram of real-time RPA (left panel) and MBDi-RPA (right panel) with a dual-labeled ORN. RNase H cleaves the hybridized dual-labeled ORN, preventing the inhibition of DNA amplification. Fluorescence is emitted from the degraded ORN. When amplification of CpG-methylated DNA is blocked by MBD proteins, no fluorescent emission is expected. F, fluorophore; Q, quencher; Star, methylation. (**C**) Specific detection of target amplification by real-time RPA. (**D** and **E**) Results of dose-dependent amplification of target DNA. Different concentrations of template DNA (CpG_10) were subjected to real-time RPA using ORN_EGFR_CG5_10_20_Probe. (**F**) Schematic diagram of the real-time MBDi-RPA procedure. (**G** and **H**) Results of real-time MBDi-RPA using MeCP2 to discriminate CpG methylation status in target DNA. CpG-methylated and -unmethylated DNA were used separately (**G**) or collectively (1:1 ratio, **H**) as template DNA. BSA was used as a negative control protein.

Fig. 5. Evaluation of real-time RPA and MBDi-RPA using model gDNA.

(**A**) Results of dose-dependent detection of target DNA in gDNA by real-time RPA. (**B**) The linear relationship between the log DNA amounts and RFU values at 20 min of the reaction. (**C**) Results of real-time MBDi-RPA using HCT116 gDNA. (**D**) Schematic diagram of the real-time MBDi-RPA procedure with commercially available CpG-methylated and -unmethylated DNA. (**E**) Results of real-time MBDi-RPA using MeCP2. CpG-methylated and -unmethylated DNA were mixed at various ratios and used as template DNA. (**F**) The linear relationship between the percentage of CpG-unmethylated DNA to CpG-methylated DNA and RFU values at 20 min of the reaction.

Table 1. Comparison of real-time methods for the detection of CpG-methylated DNA

	Time	Reagents	Advantages	Concerns
Bisulfite treatment followed by real-time MSP	4 h	Bisulfite conversion kit Real-time PCR reagent Dual-labeled probe (if necessary)	Methylation analysis of individual CpG sites High sensitivity (discrimination at several % level)	False results due to incomplete bisulfite conversion or primer misannealing DNA damage by bisulfite treatment (Shorter amplicons are preferable.) Time-consuming
MRE-digestion followed by real-time PCR	4 h	Restriction enzyme Real-time PCR reagent Dual-labeled probe (if necessary)	Cost-effective	Only 17 restriction enzymes useful for methylation analysis Limitation of restriction enzymes digestion sequences available False results due to inappropriate digestion Low sensitivity Time-consuming
Real-time MBDi-RPA	0.5 h	RPA reagent MBD protein Dual-labeled ORN (Probe) RNase H	Rapid No additional treatment of the DNA necessary	Low sensitivity (discrimination at ca. 10 % level) Further optimization may be necessary.

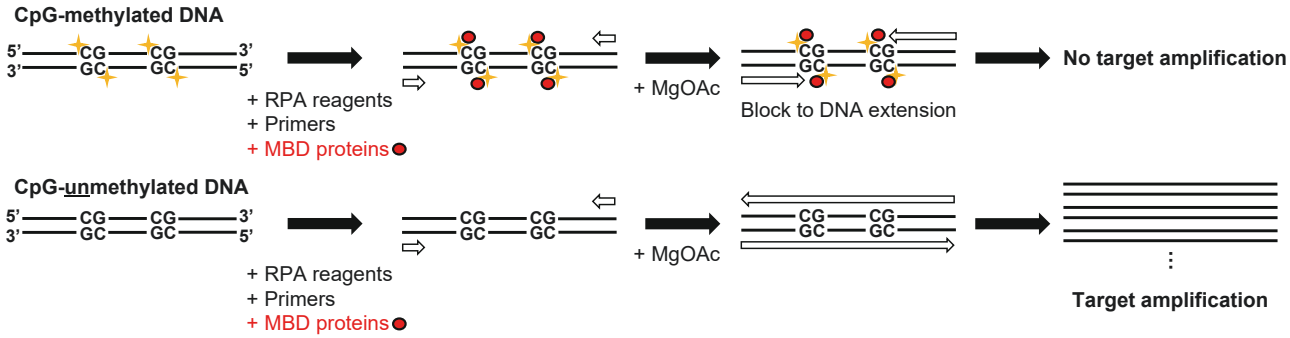
CpG-methylated DNA
5'
3'
CG
GC
3'
5'
+ RPA reagents
+ Primers
+ MBD proteins
+ MgOAc
Block to DNA extension
No target amplification
CpG-unmethylated DNA
+ RPA reagents
+ Primers
+ MBD proteins
+ MgOAc
Target amplification

Figure 1

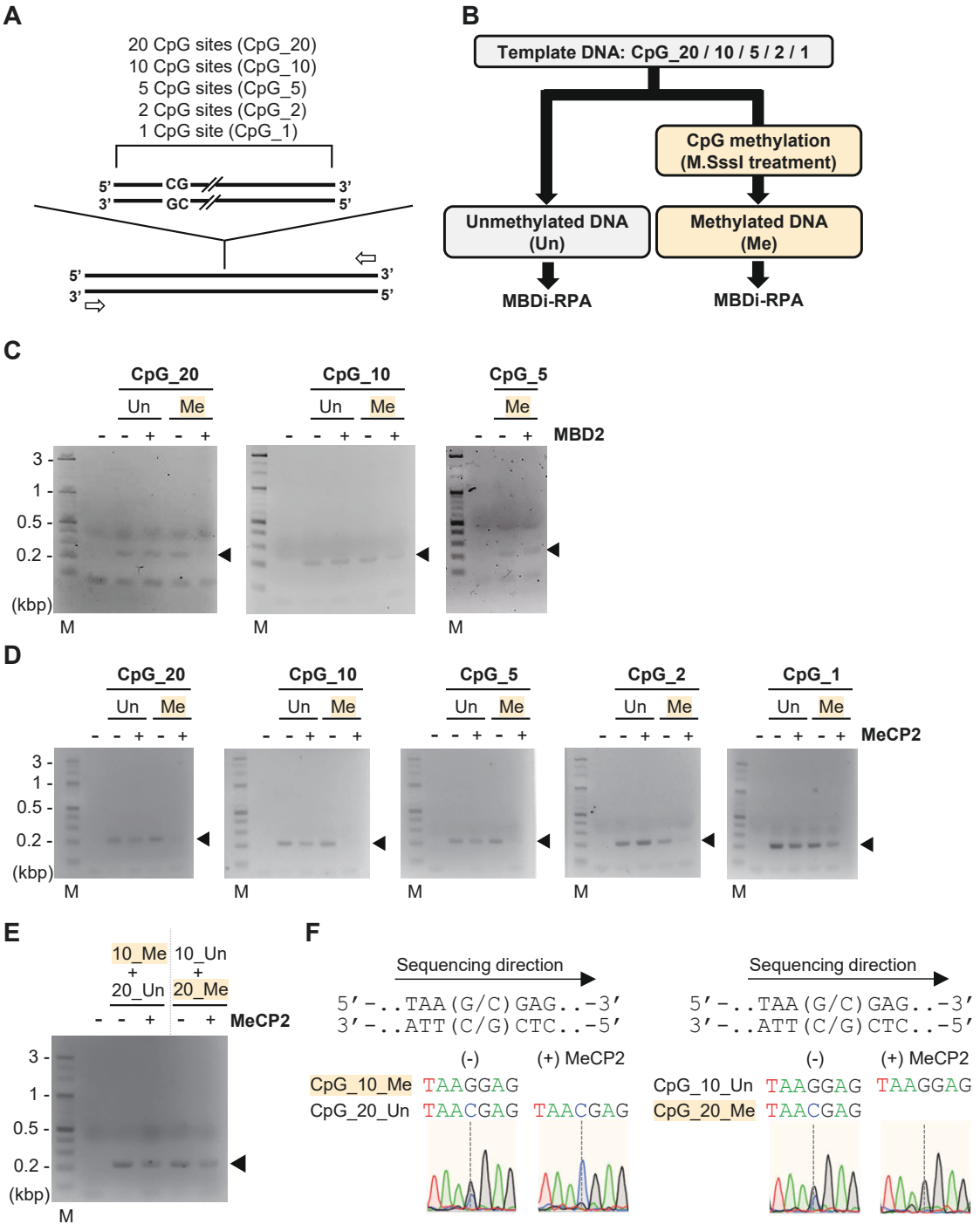
A
20 CpG sites (CpG_20)
10 CpG sites (CpG_10)
5 CpG sites (CpG_5)
2 CpG sites (CpG_2)
1 CpG site (CpG_1)
5'
3'
CG
GC
B
Template DNA: CpG_20 / 10 / 5 / 2 / 1
CpG methylation
(M.SssI treatment)
Unmethylated DNA
(Un)
Methylated DNA
(Me)
MBDi-RPA
MBDi-RPA
C
CpG_20
CpG_10
CpG_5
Un
Me
MBD2
3
1
0.5
0.2
(kbp)
M
D
CpG_20
CpG_10
CpG_5
CpG_2
CpG_1
MeCP2
E
10_Me + 20_Un
10_Un + 20_Me
MeCP2
F
Sequencing direction
5'-..TAA(G/C)GAG..-3'
3'-..ATT(C/G)CTC..-5'
(-)
(+) MeCP2
CpG_10_Me TAAGGAG
CpG_20_Un TAACGAG TAACGAG
CpG_10_Un TAAGGAG TAAGGAG
CpG_20_Me TAACGAG

Figure 2

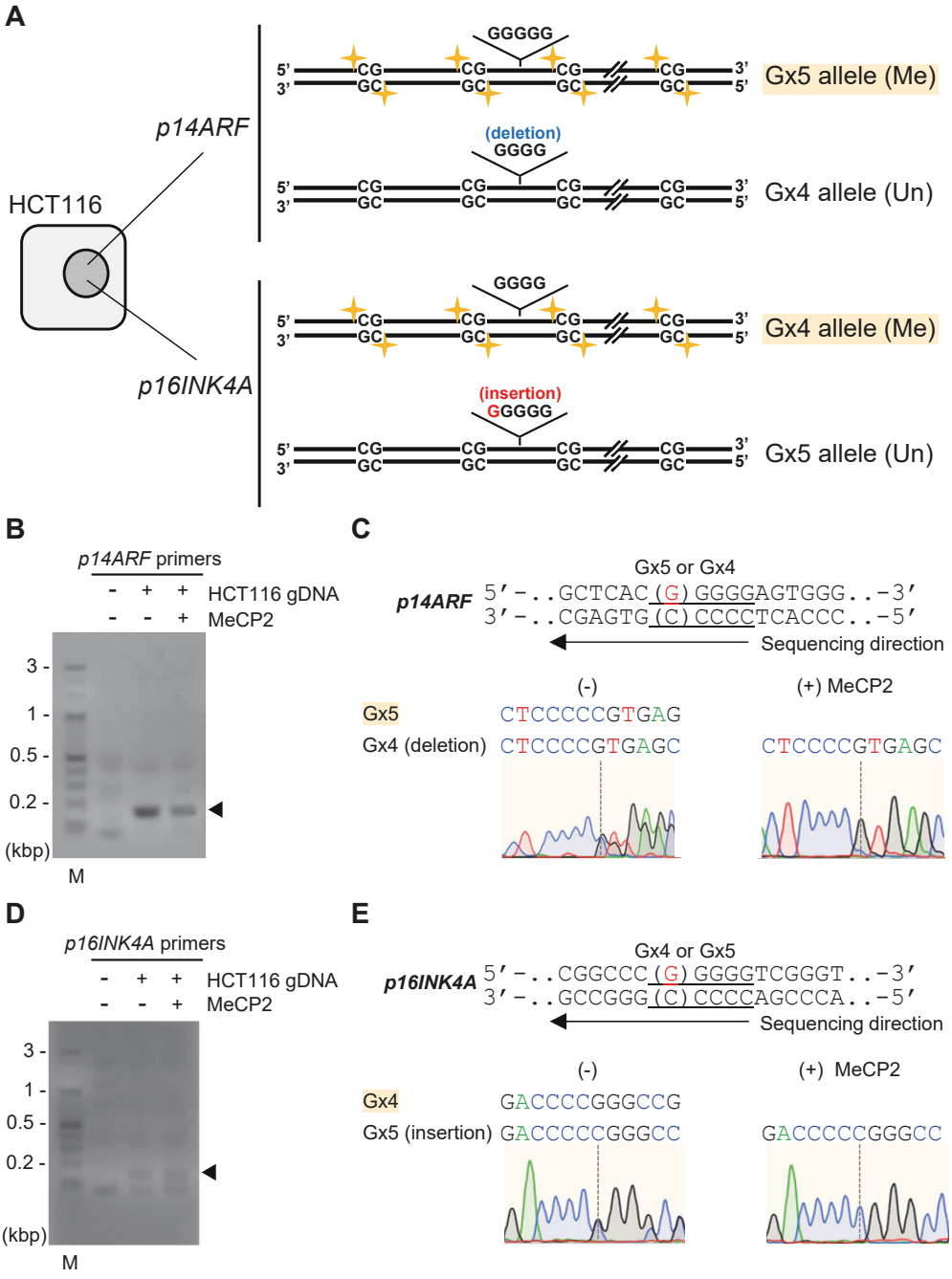
A
HCT116
p14ARF
p16INK4A
GGGGG
(deletion)
GGGG
GGGG
(insertion)
GGGGG
Gx5 allele (Me)
Gx4 allele (Un)
Gx4 allele (Me)
Gx5 allele (Un)
B
p14ARF primers
HCT116 gDNA
MeCP2
3
1
0.5
0.2
(kbp)
M
C
Gx5 or Gx4
p14ARF
5′-..GCTCAC(G)GGGGAGTGGG..-3′
3′-..CGAGTG(C)CCCCTCACCC..-5′
Sequencing direction
(-)
(+) MeCP2
Gx5
CTCCCCCGTGAG
Gx4 (deletion)
CTCCCCGTGAGC
CTCCCCGTGAGC
D
p16INK4A primers
HCT116 gDNA
MeCP2
3
1
0.5
0.2
(kbp)
M
E
Gx4 or Gx5
p16INK4A
5′-..CGGCCC(G)GGGGTCGGGT..-3′
3′-..GCCGGG(C)CCCCAGCCCA..-5′
Sequencing direction
(-)
(+) MeCP2
Gx4
GACCCCGGGCCG
Gx5 (insertion)
GACCCCCGGGCC
GACCCCCGGGCC

Figure 3

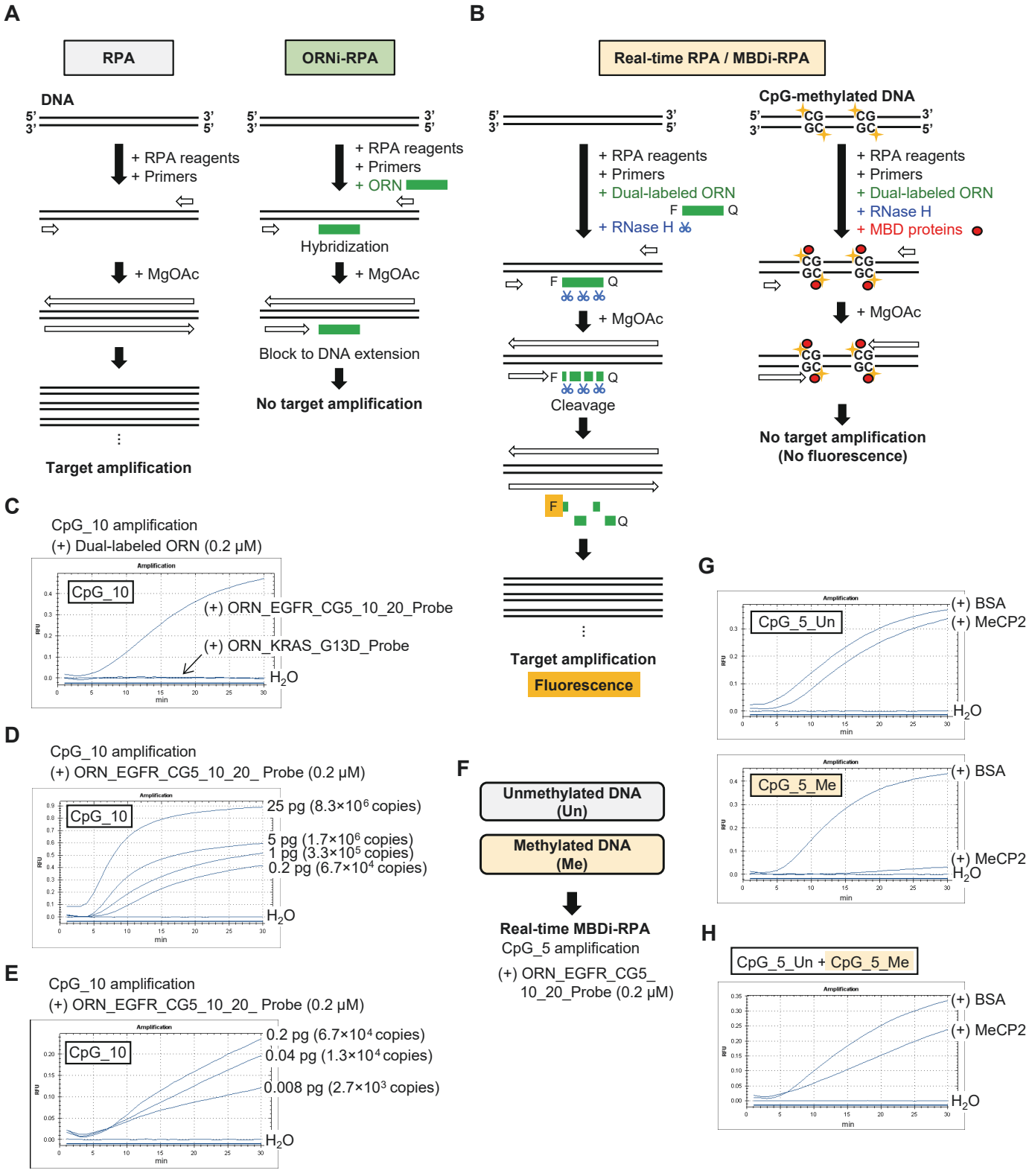
A
RPA
ORNi-RPA
DNA
5'
3'
+ RPA reagents
+ Primers
+ ORN
Hybridization
+ MgOAc
Block to DNA extension
No target amplification
Target amplification
B
Real-time RPA / MBDi-RPA
CpG-methylated DNA
+ Dual-labeled ORN
F
Q
+ RNase H
+ MBD proteins
Cleavage
No target amplification
(No fluorescence)
Target amplification
Fluorescence
C
CpG_10 amplification
(+) Dual-labeled ORN (0.2 μM)
CpG_10
(+) ORN_EGFR_CG5_10_20_Probe
(+) ORN_KRAS_G13D_Probe
H2O
D
CpG_10 amplification
(+) ORN_EGFR_CG5_10_20_ Probe (0.2 μM)
25 pg (8.3×10^6 copies)
5 pg (1.7×10^6 copies)
1 pg (3.3×10^5 copies)
0.2 pg (6.7×10^4 copies)
E
CpG_10 amplification
(+) ORN_EGFR_CG5_10_20_ Probe (0.2 μM)
0.2 pg (6.7×10^4 copies)
0.04 pg (1.3×10^4 copies)
0.008 pg (2.7×10^3 copies)
F
Unmethylated DNA (Un)
Methylated DNA (Me)
Real-time MBDi-RPA
CpG_5 amplification
(+) ORN_EGFR_CG5_10_20_Probe (0.2 μM)
G
CpG_5_Un
CpG_5_Me
(+) BSA
(+) MeCP2
H2O
H
CpG_5_Un + CpG_5_Me
RFU
min

Figure 4

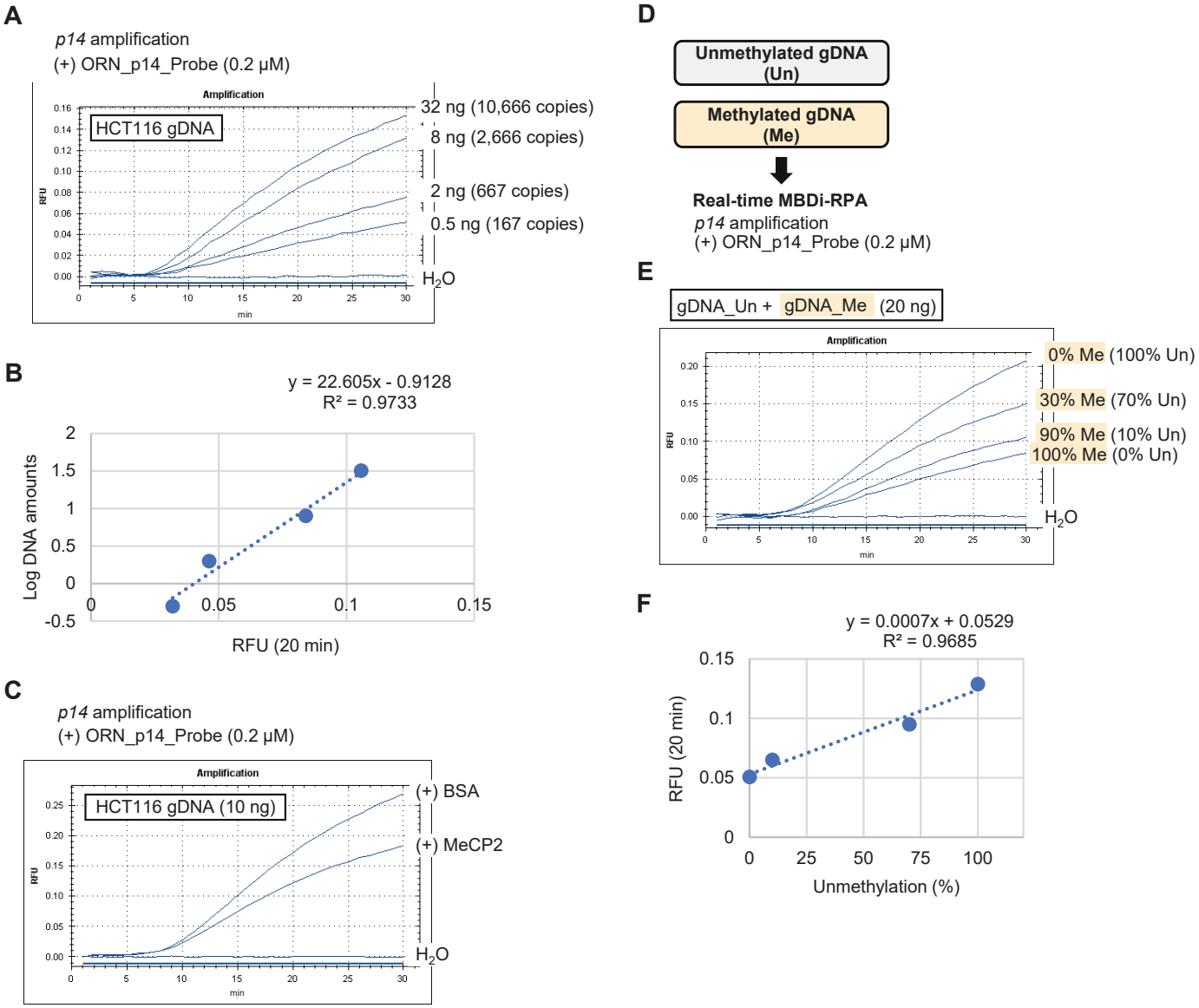
A
p14 amplification
(+) ORN_p14_Probe (0.2 μM)
Amplification
HCT116 gDNA
RFU
min
32 ng (10,666 copies)
8 ng (2,666 copies)
2 ng (667 copies)
0.5 ng (167 copies)
H2O
B
y = 22.605x - 0.9128
R² = 0.9733
Log DNA amounts
RFU (20 min)
C
p14 amplification
(+) ORN_p14_Probe (0.2 μM)
Amplification
HCT116 gDNA (10 ng)
RFU
min
(+) BSA
(+) MeCP2
H2O
D
Unmethylated gDNA (Un)
Methylated gDNA (Me)
Real-time MBDi-RPA
p14 amplification
(+) ORN_p14_Probe (0.2 μM)
E
gDNA_Un + gDNA_Me (20 ng)
Amplification
RFU
min
0% Me (100% Un)
30% Me (70% Un)
90% Me (10% Un)
100% Me (0% Un)
H2O
F
y = 0.0007x + 0.0529
R² = 0.9685
RFU (20 min)
Unmethylation (%)

Figure 5

Supporting Information

Real-time MBDi-RPA using methyl-CpG binding protein 2: a real-time detection method for simple and rapid estimation of CpG methylation status

Mina Ishidoya[1], Toshitsugu Fujita[2]*, Sadatomo Tasaka[1], Hodaka Fujii[2]

Department of Biochemistry and Genome Biology, Hirosaki University Graduate School of Medicine, 5 Zaifu-cho, Hirosaki, 036-8562 Aomori, Japan

*Correspondence:

E-mail address: toshitsugu.fujita@hirosaki-u.ac.jp (T.F.)

Table of Contents

Supplementary Table and Figure Legends

Table S1. Oligonucleotides used in this study.

Figure S1. Template plasmid DNA. DNA sequences shown below were cloned in plasmids. CpG sites are shown in red. Primer positions are highlighted in blue and green. Only the forward sequences are shown.

Figure S2. Target sequences in HCT116 gDNA. The targets were the human *CDKN2A* (*p14ARF* and *p16INK4A*) genes in HCT116 gDNA. CpG sites are underlined. Primer positions are highlighted in blue and green. The positions of allele-specific mutations (deletion and insertion of single guanine on *p14ARF* and *p16INK4A*, respectively) are indicated with red squares. Only the forward sequences are shown.

Figure S3. Real-time PCR of RPA products. (**A**) Schematic of the procedure used. (**B**) Results of real-time PCR with RPA samples. The RPA/MBDi-RPA samples shown in Fig. 2D (CpG_2) were subjected to real-time PCR.

Figure S4. Amplification of the *KRAS* gene from HCT116 gDNA by real-time RPA. (**A**) Schematic diagram of the human *KRAS* gene in HCT116 gDNA. (**B**) The target *KRAS*

sequence is shown. Primer positions are highlighted in blue and green. The allele-specific G13D mutation is shown in red. Only the forward sequence is shown. (**C**) ORN_KRAS_G13D_Probe. (**D**) RPA in the presence of a dual-labeled ORN and RNase H. The amplified target DNA is indicated by an arrowhead. M, molecular weight marker. (**E**) Specific detection of target amplification by real-time RPA.

Figure S5. Amplification of CpG_10 by real-time RPA. (**A**) The target CpG_10 sequence is shown. Primer positions are highlighted in blue and green. The ORN position is shown in gray. CpG sites are shown in red. (**B**) Amplicons of real-time RPA shown in Fig. 4D. The amplified target DNA is indicated by an arrowhead. M, molecular weight marker.

Figure S6. Potential discrimination of a single-nucleotide mutation by real-time RPA. (**A** and **C**) *KRAS* amplification by real-time RPA with ORN_KRAS_G13D_Probe. Fluorescence was emitted more strongly from HCT116 gDNA with the *KRAS* G13D mutation. (**B** and **D**) Amplicons of real-time RPA. The amplified target DNA is indicated by arrowheads. M, molecular weight marker.

Figure S7. Real-time RPA in the presence or absence of an irrelevant protein. Results of real-time MBDi-RPA with an irrelevant protein (BSA).

Figure S8. Amplification of the *p14ARF* gene by real-time RPA and MBDi-RPA. (**A**) The target *p14ARF* sequence is shown. Primer positions are highlighted in blue and green. The ORN position is shown in gray. CpG sites are shown in red. (**B**) Detection of target amplification by real-time RPA. (**C**) RPA in the presence of various concentration of MeCP2. The amplified target DNA is indicated by an arrowhead. M, molecular weight marker. (**D**) Results of DNA sequencing analysis. RPA and MBDi-RPA amplicons shown in (**C**) were sequenced using a reverse primer. See also Fig. 3A and S2 about the *p14ARF* gene in HCT116.

Table S1

Categories	Name	Sequence (5'→3')	Experiments	Number
ORN (Probe)	ORN_EGFR_CG5_10_20_Probe	TAMRA-cccacuagcuguauuguuuaac-FAM	Figs. 4 and S7	R97
	ORN_KRAS_G13D_Probe	TAMRA-gugacguaggcaagagugc-FAM	Figs. S4 and S6	R94
	ORN_p14_Probe	TAMRA-cgccgcuguggcccucgugc-FAM	Figs. 5 and S8	R104
Primer	EGFR-RPA-L858-F	TGGCAGCCAGGAATGTACTGGTGAAAACACTGCAGCATG	Figs. 2, 4, S5, and S7	28364
	EGFR-RPA-L858-R3	CAGAATGTCTGGAGAGCATCCTCCCCTGCATG	Figs. 2, 4, S5, and S7	28368
	p14-RPA-F3	AGAACATGGTGCGCAGGTTCTTGGTGACCCTC	Figs. 3B, 5 and S8	28876
	p14-RPA-R3	GCTGCCCTAGACGCTGGCTCCTCAGTAGCATC	Figs. 3B, 5 and S8	28877
	p16-RPA-F6	GGGAGCAGCATGGAGCCTTCGGCTGACTGGCTGGC	Fig. 3D	28878
	p16-RPA-R6	CCGCTGCAGACCCTCTACCCACCTGGATCGGCCTC	Fig. 3D	28879
	KRAS-RPA-G12-F	TAGTGTATTAACCTTATGTGTGACATGTTCTAAT	Figs. S4 and S6	28318
	KRAS-RPA-G12-R2	GTATCAAAGAATGGTCCTGCACCAGTAATATGC	Figs. S4 and S6	28905
	hEGFR-Exon21-F12	TGCAGCATGTCAAGATCACA	Fig. S3B	29027
	hEGFR-Exon21-R12	CCTCCCCTGCATGTGTTAAA	Fig. S3B	29028

Fig. S1

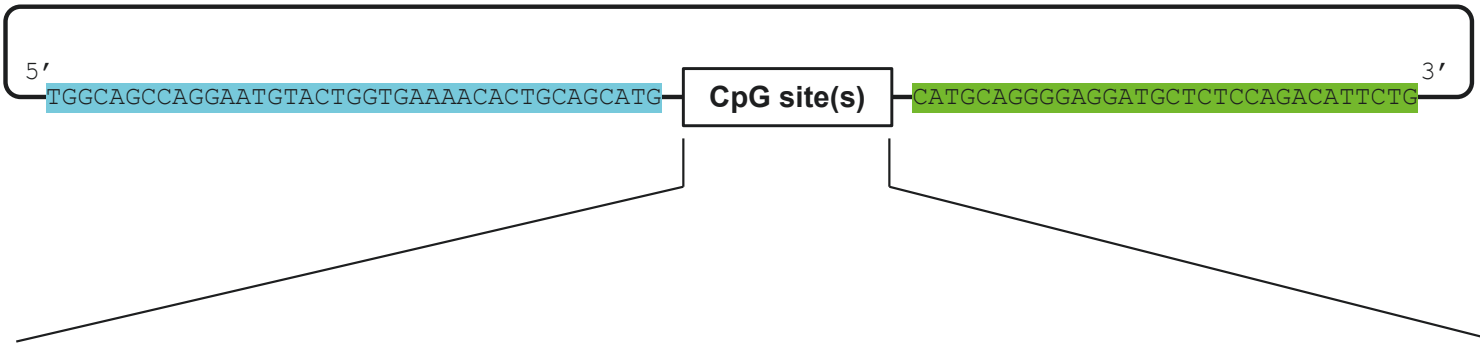

CpG_20

5′-..CGGGCGAAACGGCTGCGTGCGGAAGCGAACGAATACCGTGCAGACGGACGCAACGTAACGAGGTCGCTTTCGGTCGGCCAGCGTTTTCGTGACACCACGGACCACGCTGCG..-3′

CpG_10

5′-..CGGGCCAAACGGCTGGGTGCGGAAGAGAACGAATACCATGCAGACGGAGGCAACGTAAGGAGGTCGCTTTAGGTCGGCCAGCGTTTTCCTGACACCACGGACCAGGCTGCC..-3′

CpG_5

5′-..CGGGCCAAACTGCTGGGTGCGGAAGAGAAAGAATACCATGCAGACGGAGGCAAAGTAAGGAGGTCGCTTTAGGTCAGCCAGCGTTTTCCTGACACCAGGGACCAGGCTGCC..-3′

CpG_2

5′-..CGGGCCAAACTGCTGGGTGCGGAAGAGAAAGAATACCATGCAGAAGGAGGCAAAGTAAGGAGGTGGCTTTAGGTCAGCCAGCATTTTCCTGACACCAGGGACCAGGCTGCC..-3′

CpG_1

5′-..CTGGCCAAACTGCTGGGTGCGGAAGAGAAAGAATACCATGCAGAAGGAGGCAAAGTAAGGAGGTGGCTTTAGGTCAGCCAGCATTTTCCTGACACCAGGGACCAGGCTGCC..-3′

Fig. S2

p14ARF

5′-..G**CG**AGAACATGGTG**CG**CAGGTTCTTGGTGACCCTC**CG**GATT**CG**G**CGCGCG**TG**CG**GCC**CG**C**CGCG**AGTGAGGGTTTT**CG**TGGTTCACATCC**CG**
CGGCTCA**CG**GGGGGAGTGGGCAG**CG**CCAGGGG**CG**CC**CG**C**CG**CTGTGGCCCT**CG**TGCTGATGCTACTGAGGAGCCAG**CG**TCTAGGGCAGCAGC..-3′

Gx5 or Gx4

p16INK4A

Gx4 or Gx5

5′-..G**CG**GGGAGCAGCATGGAGCCTT**CG**GCTGACTGGCTGGCCA**CG**GC**CGCG**GCCC**CG**GGGTCGGGTAGAGGAGGTG**CG**GG**CG**CTGCTGGAGG**CG**GG
GG**CG**CTGCCCAA**CG**CAC**CG**AATAGTTA**CG**GT**CG**GAGGCCGATCCAGGTGGGTAGAGGGTCTGCAG**CG**GGAG..-3′

Fig. S3

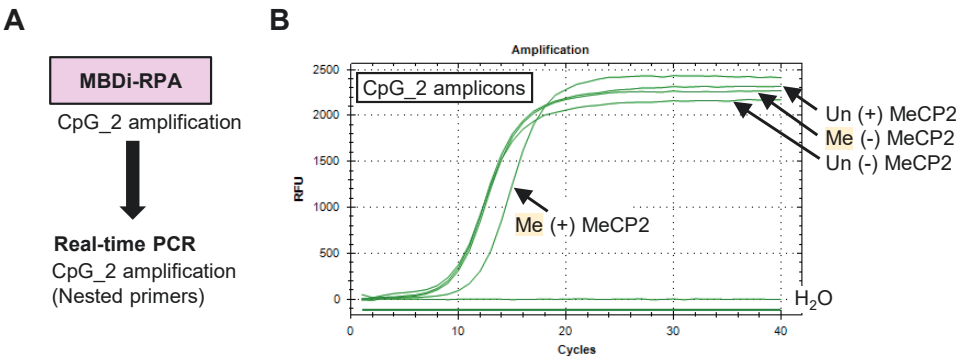
A
MBDi-RPA
CpG_2 amplification
Real-time PCR
CpG_2 amplification
(Nested primers)
B
Amplification
CpG_2 amplicons
RFU
2500
2000
1500
1000
500
0
0
10
20
30
40
Cycles
Un (+) MeCP2
Me (-) MeCP2
Un (-) MeCP2
Me (+) MeCP2
H2O

Fig. S4

A

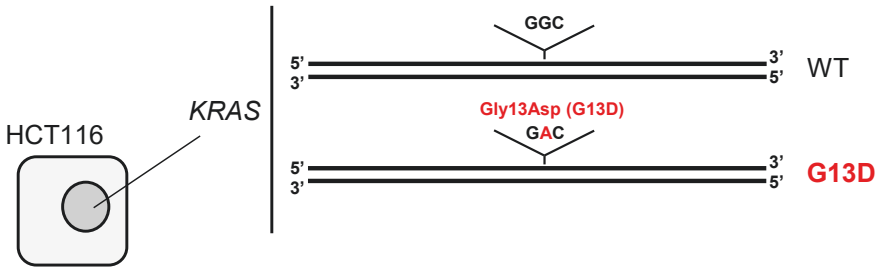

B

KRAS

5′-..TGATAGTGTATTAACCTTATGTGTGACATGTTCTAATATAGTCACATTTTCATTATTTTTA
TTATAAGGCCTGCTGAAAATGACTGAATATAAACTTGTGGTAGTTGGAGCTGGTG(G/A)CGTAGG
CAAGAGTGCCTTGACGATACAGCTAATTCAGAATCATTTTGTGGACGAATATGATCCAACAATAGA
GGTAAATCTTGTTTTAATATGCATATTACTGGTGCAGGACCATTCTTTGATACAGA..-3′

C

WT 5′-..TGGTGGCGTAGGCAAGAGTGCCT..-3′

G13D 5′-..TGGTGACGTAGGCAAGAGTGCCT..-3′

5′(TAMRA)-gugacguaggcaagagugc-(FAM)3′ **ORN_KRAS_G13D_Probe**

D

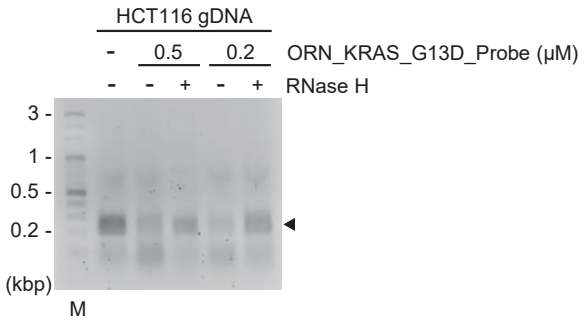

E

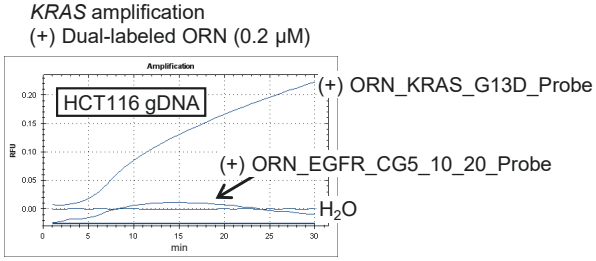

Fig. S5

A

CpG_10

5′-..GATTGGCAGCCAGGAATGTACTGGTGAAAACACTGCAGCATGTCAAGATCACAGATTTTGGGCGGGCCAAACGGCT
GGGTGCGGAAGAGAACGAATACCATGCAGACGGAGGCAACGTAAGGAGGTCGCTTTAGGTCGGCCAGCGTTTTCCTGACAC
CACGGACCAGGCTGCCTTCCCACTAGCTGTATTGTTTAACACATGCAGGGGAGGATGCTCTCCAGACATTCTGGGT..-3′

5′(TAMRA)-cccacuagcuguauuguuuaac-(FAM)3′

ORN_EGFR_CG5_10_20_Probe

B

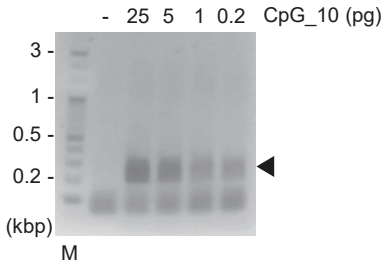

Fig. S6

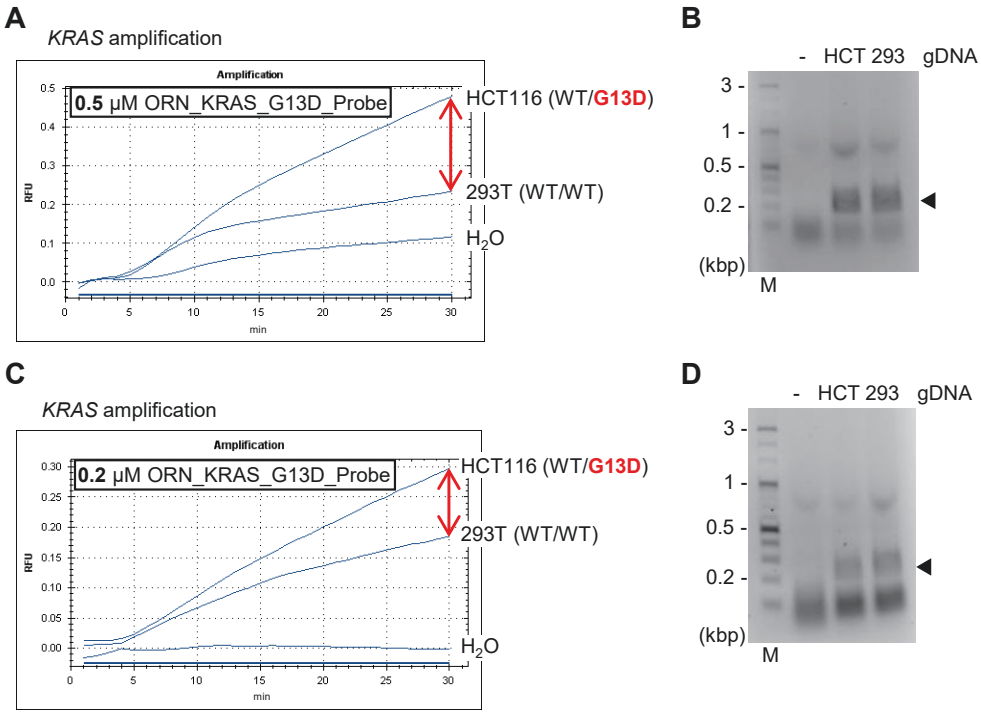
A
KRAS amplification
Amplification
0.5 µM ORN_KRAS_G13D_Probe
HCT116 (WT/G13D)
293T (WT/WT)
H2O
RFU
min
B
- HCT 293 gDNA
3 -
1 -
0.5 -
0.2 -
(kbp)
M
C
KRAS amplification
Amplification
0.2 µM ORN_KRAS_G13D_Probe
HCT116 (WT/G13D)
293T (WT/WT)
H2O
RFU
min
D
- HCT 293 gDNA
3 -
1 -
0.5 -
0.2 -
(kbp)
M

Fig. S7

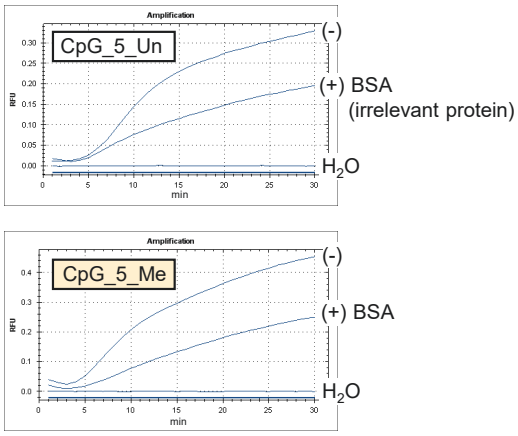
Amplification
CpG_5_Un
RFU
min
(-)
(+) BSA
(irrelevant protein)
H2O
Amplification
CpG_5_Me
RFU
min
(-)
(+) BSA
H2O

Fig. S8

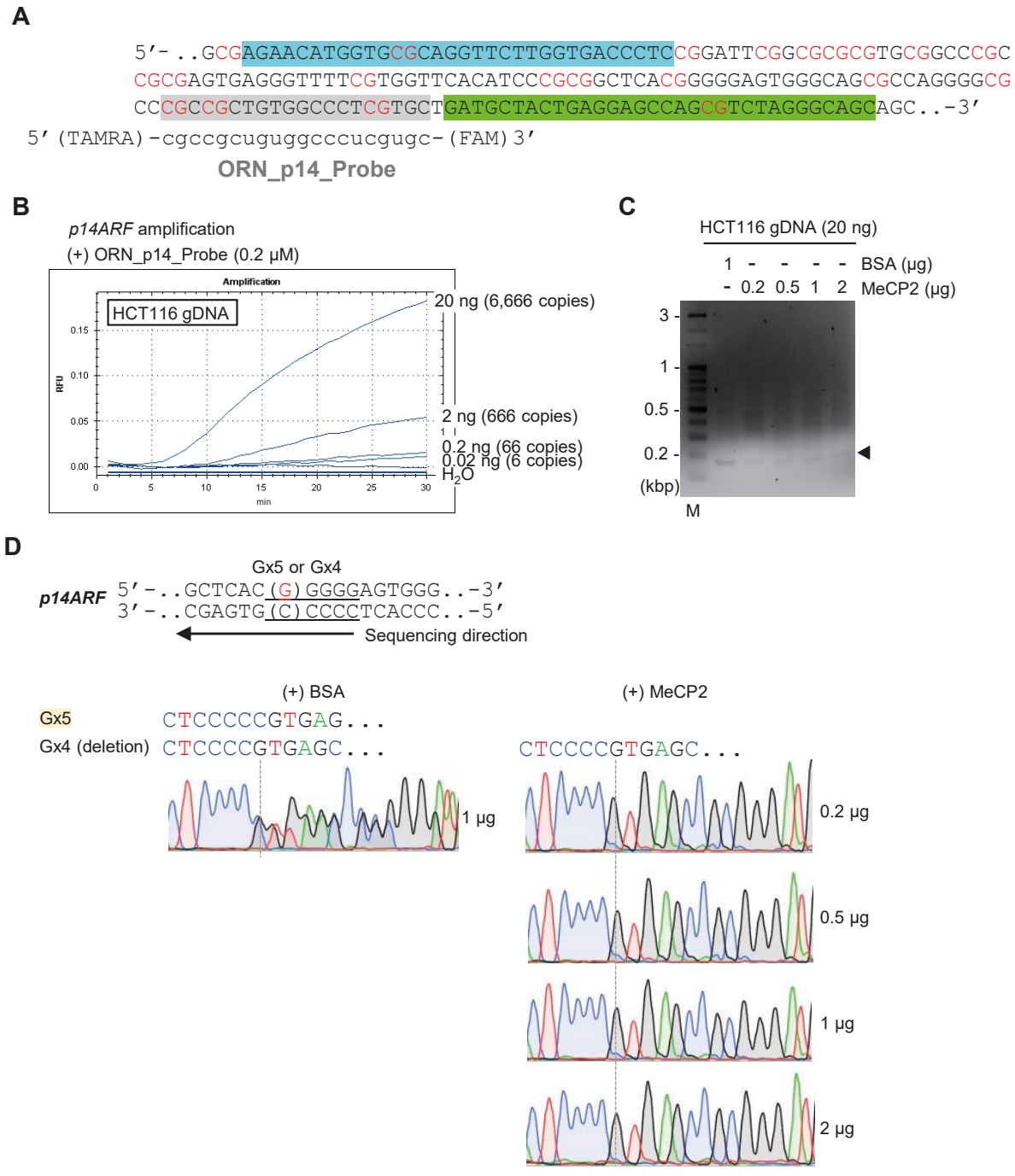
A
5′- ..GCGAGAACATGGTGCGCAGGTTCTTGGTGACCCTCCGGATTCGGCGCGCGTGCGGCCCGC
CGCGAGTGAGGGTTTTCGTGGTTCACATCCCGCGGCTCACGGGGGAGTGGGCAGCGCCAGGGGCG
CCCGCCGCCTGTGGCCCTCGTGCTGATGCTACTGAGGAGCCAGCGTCTAGGGCAGCAGC..-3′
5′(TAMRA)-cgccgcuguggcccucgugc-(FAM)3′
ORN_p14_Probe
B
p14ARF amplification
(+) ORN_p14_Probe (0.2 μM)
Amplification
HCT116 gDNA
RFU
min
20 ng (6,666 copies)
2 ng (666 copies)
0.2 ng (66 copies)
0.02 ng (6 copies)
H2O
C
HCT116 gDNA (20 ng)
1 - - - - BSA (μg)
- 0.2 0.5 1 2 MeCP2 (μg)
3
1
0.5
0.2
(kbp)
M
D
Gx5 or Gx4
p14ARF 5′-..GCTCAC(G)GGGGAGTGGG..-3′
3′-..CGAGTG(C)CCCCTCACCC..-5′
Sequencing direction
(+) BSA
(+) MeCP2
Gx5 CTCCCCCGTGAG...
Gx4 (deletion) CTCCCCGTGAGC...
CTCCCCGTGAGC...
1 μg
0.2 μg
0.5 μg
1 μg
2 μg